Catalysis Science & Technology

Accepted Manuscript

This article can be cited before page numbers have been issued, to do this please use: C. Liu, W. Guo, J. Chen, J. Zou, Z. Wang and L. Wu, *Catal. Sci. Technol.*, 2020, DOI: 10.1039/D0CY01721C.

ROYAL SOCIETY OF CHEMISTRY

rsc.li/catalysis

View Article Online
DOI: 10.1039/D0CY01721C

ARTICLE

Ultrathin ZnTi-LDH nanosheets for photocatalytic aerobic oxidation of aniline based on coordination activation

Received 00th January 20xx,
Accepted 00th January 20xx

DOI: 10.1039/x0xx00000x

Cheng Liu,[a] Wei Guo,[a], Jinsong Chen,[a], Junhua Zou,[a], Zhiwen Wang,[a] and Ling Wu*[a]

In this work, ZnTi-LDH nanosheets with several monolayers thickness were prepared as photocatalysts for aerobic oxidation of aniline to yield nitrosobenzene under visible light irradiation. UV–vis DRS, in situ FTIR and XPS results jointly revealed that aniline molecules were efficiently chemisorbed and activated on ZnTi-LDH to form surface coordination active species, improving visible light absorption and inducing the photocatalytic reaction. The surface OH groups on ZnTi-LDH as the Brønsted base sites facilitated the reductive deprotonation of aniline to form anilino anion, which was a key step in promoting aniline oxidation. ESR and XPS data suggested that oxygen vacancies (OVs) were formed due to the interaction between exposed OH groups and aniline molecules. The OVs as the centers to capture photoelectrons achieve the reduction of oxygen molecules to $\bullet O_2^-$ radicals, which further oxidize anilino species to produce nitrosobenzene. Finally, a possible mechanism was proposed to reveal the photocatalytic process based on surface coordination activation theory.

1. Introduction

Nitrosobenzene as a highly valuable intermediate undergoes a variety of organic synthesis reactions, including additions, isomerizations, oxidations, reductions as well as ene reactions. [1,2] In the past, nitrosobenzene was synthesized by oxidation of aniline using peracids as oxidizing agents, which were corrosive and unstable.[3-5] Recent developments of heterogeneous catalytic oxidation have attracted much attention, but those processes require expensive hydrogen peroxide (H_2O_2) as the oxidant.[6,7] Considering the viewpoint of environmentally friendly chemistry, the catalytic oxidation with oxygen (O_2) as the oxidant is subsequently developed.[8,9] However, high temperature and high pressure needed in those reactions cause very low selectivity to nitrosobenzene. Consequently, it is well worth finding a novel and economical strategy to achieve the oxidation of aniline to nitrosobenzene under mild conditions using oxygen as the oxidant.

Much work so far has focused on photocatalytic organic transformation, a green and sustainable process, in which organic reaction could be initiated by light irradiation under mild conditions.[10-12] So photocatalysis is a promising candidate for the selective aerobic oxidation of aniline to nitrosobenzene. Recently, it was demonstrated in three studies about photocatalytic aerobic oxidation of aniline under UV irradiation.[13-15] But nitrosobenzene is hardly detected in those processes as a result of the forming of azobenzene. Afterwards, selective photocatalytic oxidation of aniline to nitrosobenzene over Pt/TiO_2 was reported.[16] However, Pt/TiO_2 catalyst was prepared under a harsh condition and used an expensive noble metal (Pt). Therefore, it is desired to explore efficient catalysts for selective photocatalytic oxidation of aniline to nitrosobenzene in an economic and convenient way.

Considerable research efforts have been devoted to ultrathin two dimensional (2D) materials due to high specific surface area, unique surface states, abundant active sites and other distinctive physicochemical properties.[17-20] In our previous work, a series of ultrathin 2D nanosheets such as HNb_3O_8,[21] Bi_2MoO_6,[22,23] $H_{1.4}Ti_{1.65}O_4{\cdot}H_2O$[24-27] as well as BiOCl[28] were developed for photocatalytic selective organic transformation. It was revealed in these studies that the ultrathin 2D material is an ideal model to explore the interaction between reactants and catalysts, which probably provides an in-depth understanding of the photocatalytic reaction mechanism at a molecular level.

Layered double hydroxides (LDHs) as an important class of 2D materials have been widely applied in photocatalysis, catalysis, biomedical science, electrochemistry and so on.[29-32] LDHs have become promising photocatalysts owing to several outstanding advantages, including abundant surface hydroxyl (OH) groups, the unique structure, uniform distribution of different metal cations, flexible tunability and high chemical stability. In photocatalysis region, most of literatures about LDHs focus on water splitting,[33-35] CO_2 reduction[36,37] and degradation of pollutant.[38] However, small amount of work has been reported on the photocatalytic organic transformation by LDHs.[39,40] Recently, our research group has reported photocatalytic selective oxidation benzyl alcohol over Au-Pd/MgAl-LDH and ZnTi-LDH under visible light irradiation.[41,42] Both literatures highlight the interaction between the basic

[a] State Key Laboratory of Photocatalysis on Energy and Environment, Fuzhou University, Fuzhou 350116, P.R. China. E-mail: wuling@fzu.edu.cn

Electronic Supplementary Information (ESI) available: [details of any supplementary information available should be included here]. See DOI: 10.1039/x0xx00000x

sites on the surface of LDHs and reactant molecules. It was demonstrated by Hirai et al. that Pt/TiO_2 possessed the excellent photocatalytic performance on aniline oxidation to nitrosobenzene because the Pt particles with high electron density behaved as Lewis base sites to achieve reductive deprotonation of aniline, which was the rate determining step to oxidation of aniline.[16] Following this thought, the function of the basic sites was further emphasized in our two reported studies. [43,44] Therefore, whether surface OH groups of LDHs as the Brønsted base sites could facilitate the reductive deprotonation of aniline to increase catalytic activity or not?

Herein, we fabricated ZnTi-LDH nanosheets with 7~8 monolayers thickness for selective photocatalytic aerobic oxidation of aniline to nitrosobenzene under visible light irradiation. The three kinds of ZnTi-LDHs with different molar ratio of Zn^{II}/Ti^{IV} were prepared by varying dosage of $TiCl_4$. The unique ultrathin structure for ZnTi-LDH was exhibited by FESEM, TEM and AFM. The differences of the three kinds of ZnTi-LDHs on specific surface area, light absorption, and the amount of surface OH groups were revealed by BET, UV–vis DRS and FTIR, respectively. The interaction between OH groups on the surface of ZnTi-LDH and aniline molecules was investigated by UV–vis DRS, in situ FTIR and XPS. The presence of oxygen vacancies produced by the interaction between ZnTi-LDH and aniline molecules was verified by ESR and XPS. The generation of superoxide radical ($\bullet O_2^-$) as the active oxidative species further was characterized by ESR combined with DMPO. Finally, a possible mechanism was proposed at a molecule level to illustrate photocatalytic progress of oxidation of aniline to nitrosobenzene based on surface coordination activation theory.

2. Experimental

2.1 Reagents and chemicals. Zinc nitrate hexahydrate ($Zn(NO_3)_2{\cdot}6H_2O$, 99%), Urea (CH_4N_2O, 99%), Titanium tetrachloride ($TiCl_4$, 98%), Acetonitrile (CH_3CN, 99%), Aniline (C_6H_7N, 99%), Ntrobenzene ($C_6H_5NO_2$, 99%) were purchased from Sinopharm Chemical Reagent Co., Ltd. (Shanghai, China). Nitrosobenzene (C_6H_5NO, 97%) and Azobenzene ($C_{12}H_{10}N_2$, 97%) were purchased from Sigma-Aldrich Co., Ltd. and Alfa Aesar China Co., Ltd., respectively. All these chemicals were used as received without a further purification.

2.2 Catalysts preparation. ZnTi-LDH was prepared by an improved co-precipitation preparation method by Duan et al.[45] Firstly, 2.38 g of $Zn(NO_3)_2{\cdot}6H_2O$ and 3 g of urea were dissolved in 70 mL of deionized water under stirring for 5 min to ensure complete dissolution. Then, 0.44 mL of $TiCl_4$ was quickly added into the mixed solution under continuously stirring for 1 h. The resulting solution was subsequently transferred to a Teflon-lined stainless steel autoclave and then heated at 130 °C for 48 h. The white precipitate was collected by centrifugation, washed several times with deionized water to remove residual ions and then dried in an oven at 60 °C for 24 h. This product was denoted as ZT-2/1, meaning ZnTi-LDH with a Zn^{II}/Ti^{IV} molar ratio of 2:1. Similarly, ZT-4/1 and ZT-6/1 were also prepared using the same procedure by varying dosage of $TiCl_4$.

2.3 Materials characterization. The X-ray diffraction (XRD) patterns were collected on a Bruker D8 Advance X-ray diffractometer with Cu Kα radiation (λ = 0.15406 nm). Hitachi SU8010 field-emission scanning electron microscopy (FESEM) was used to obtain the morphologies of the prepared samples. Transmission electron microscopy (TEM) image and higher-resolution transmission electron microscopy (HRTEM) image were characterized using a FEI Talos field emission transmission electron microscope at an accelerating voltage of 200 kV. A tapping-mode atomic force microscope (AFM, Bruker Dimension Icon) was used to determine the thickness of the samples. The Brunauer–Emmett–Teller (BET) surface area determination and Barret–Joyner–Halender (BJH) pore volume and size analysis were carried out by nitrogen adsorption/desorption isotherms at 77 K on an Autosorb-1C-TCD physical adsorption instrument (American Quantach-rome) using a Micrometrics ASAP 2020 system. Ultraviolet–visible diffuse reflectance spectra (UV–vis DRS) was obtained on an Agilent Cary 500 UV–vis spectrophotometer using Barium sulfate as background. The Fourier transform infrared (FTIR) spectra were performed on a Nicolet IS50 Fourier transform infrared spectrometer at a resolution of 4 cm^{-1}. And the prepared LDHs were pressed into KBr discs with a weight ratio of sample to KBr of 1:50. X-ray photoelectron spectroscopy (XPS) analysis was measured on a PHI Quantum 2000 XPS system with Al Ka irradiation as the excitation source. Electron spin resonance (ESR) spectra were collected on a Bruker A300 spectrometer**.** The light intensity was measured by PL-MW2000 optical power meter (Beijing PerfectLight Technology Ltd, China).

2.4 Electrochemistry measurement. The working electrode was prepared on fluorine-doped tin oxide (FTO) glass. Firstly, the FTO surface was covered by Scotch tape, leaving a circular region exposed. Then, the exposed circular region on the FTO was coated with 15 μL of the slurry, which was obtained by sonicating the mixture of 5 mg of the sample and 0.5 mL of DMF for 1 h. After dried at 60 °C for 2 h, the attached Scotch tape was torn off to leave a circular region containing the sample. The circular region was isolated with epoxy resin and the exposed area of the electrode was 0.25 cm^2. The electrochemical measurements were performed in a conventional three electrode cell in a 0.2 M of Na_2SO_4 aqueous solution (pH = 6.8), using a Pt plate as the counter electrode and a saturated Ag/AgCl electrode as the reference electrode. The Mott-Schottky plots were performed at three different frequencies (500 kHz, 1000 kHz and 1500 kHz) on a Bio-Logic SAS (SP-300) workstation. The photocurrent measurements were conducted on a CHI660D workstation using a 300 W Xe lamp with a 400 nm cut-off filter.

2.5 Simulated in situ FTIR measurement. The in situ FTIR spectra of aniline (AL) adsorbed on the samples were carried out on a Nicolet IS50 Fourier transform infrared (FTIR) spectrometer at a resolution of 4 cm^{-1}. Each spectrum was obtained by a total of 64 scans. Firstly,

20 mg of powder sample was pressed into a self-supporting IR disk with the size of 18 mm diameter, and then the disk was placed into the sample holder which could be moved vertically along a quartz tube of the cell. The sample disk was treated under dynamic vacuum (6×10^{-2} hPa) at 150 °C for 4 h to remove surface absorbed gas before initiating the first FTIR measurement (Degassing stage). After the sample cooling to room temperature, 10 μL of AL was spiked into the cell with a syringe via the septum. Half an hour later, the second FTIR measurement of the sample was collected (Physical and chemical adsorption stage). The physically absorbed AL was removed by a further evacuation at 150 °C for 3 min under 6×10^{-2} hPa, and then the third FTIR measurement of the sample was taken (Chemical adsorption stage).

2.6 Photocatalytic activity test. The photocatalytic oxidation of aniline (AL) to nitrosobenzene (NSB) with oxygen was carried out as follows. Firstly, a total of 20 mg of catalyst, 0.026 mmol of AL, and 1.0 mL of acetonitrile were added in a 10 mL of Pyrex glass reaction tube connected with a filled oxygen balloon. Then the tube was stirred for 30 min to ensure the catalyst blend evenly in the solvent. Subsequently the suspension was irradiated by a 300 W Xe lamp (Beijing Perfectlight Co. Ltd., PLS-SXE300D) with a 400 nm cut-off filter. The distance between Xe lamp and reaction tube is 6.5 cm, and the corresponding irradiation intensity is 522 mW/cm^2. The thermostat bath was used to control reaction temperature at 25 °C. After irradiation for 4 h, the catalyst was completely removed by centrifuging the mixture to gain the remaining solution, which was finally analyzed by an Agilent gas chromatograph (GC-6898N). The conversion of AL and the selectivity to NSB were defined as the follows:

Conversion (%) = $[(C_0 - C_{AL})/ C_0] \times 100$

Selectivity (%) = $[C_{NSB}/ (C_0 - C_{AL})] \times 100$

Where C_0 is the initial concentration of aniline.

The details of the GC analysis: The remaining solution was determined by an Agilent GC-6898N with FID detector. Agilent HP-5 (15m × 0.530mm) was used as a separation column. The carrier gas was Helium (99.999%) at the rate of 5.6 mL/min. The temperatures of the injector and detector were respectively set as 300°C and 270°C. The injection volume was 10 μl. The column temperature was programmed from 40°C to 160°C at 20°C /min, and then holding 10.5 min at 160°C.

3. Results and Discussion

Fig. 1 illustrates the powder XRD patterns for the three kinds of ZnTi-LDHs with different Zn^{II}/Ti^{IV} molar ratio, including ZT-2/1, ZT-4/1 and ZT-6/1. The patterns display reflections of (0 0 3), (0 0 6), (0 0 9), (1 0 0), (1 0 1), (0 1 2), (1 1 0) and (1 1 3), which belong to typical LDH materials.[46] It can also be clearly noted that the diffraction peaks especially for (0 0 3) are sharp and intense, indicating highly crystalline nature of the prepared samples. What's more, the basal interlayer reflection ($2\theta \approx 13.4°$, d_{003} = 0.66 nm) of ZnTi-LDH shows a little shift to higher scattering angle compared with that of MgAl-LDH ($2\theta \approx 11.7°$, d_{003} = 0.75 nm) reported in previous work,[44] indicating the decrease of the basal interlayer distance. This result suggests that the electrostatic interaction between inorganic layer and guest carbonate in hydrotalcite materials is strengthened because trivalent metal (Al^{3+}) in MgAl-LDH is replaced by tetravalent metal (Ti^{4+}) for ZnTi-LDH.[45]

Field-emission scanning electron microscopy (FESEM) and transmission electron microscopy (TEM) were used to obtain the morphology and structure of the LDH sample. The FESEM image, shown in Fig. 2A, reveals that the prepared ZnTi-LDHs consist of two-dimensional thin nanoflakes. The rough surface of hierarchical structure contributes to the contact between catalysts and reactants, which plays an important role in improvement of catalytic performance. It is further confirmed by TEM image in Fig. 2B that the hierarchical structure of the sample consists of ultrathin nanosheets with lateral dimension of 500~700 nm. As can be seen from HRTEM image in Fig. 2C, the interplanar spacing of the sample is 0.25 nm, which is consistent with the calculated result (d_{009} = 0.25 nm) based on the XRD results. In addition, the thickness of the ZnTi-LDH nanosheets measured by atomic force microscope (AFM) in Fig. 2D-F is approximately 4.7~5.2 nm, which can be considered as the 7~8 monolayers thickness according to the interlayer spacing of 0.66 nm from XRD data.

The specific surface area and porosity of the ZnTi-LDHs were invstigated by the low temperature nitrogen adsorption-desorption. The N_2-sorption data in Fig. S1A shows a type IV isotherm with a H3-type hysteresis loop for the ZnTi-LDHs, which demonstrates that the prepared ZnTi-LDHs are mesoporous materials. The corresponding wide distribution of pore size in Fig. S1B further confirms that pore width of the samples is distributed in 6–7 nm, most likely resulting from use of urea as the template during the hydrothermal synthesis. Meanwhile, the specific surface area of ZT-2/1, ZT-4/1, and ZT-6/1 were measured to be 129.07 m^2/g, 86.79 m^2/g and 48.08 m^2/g, respectively. Furthermore, the optical property of prepared catalysts was analyzed by ultraviolet–visible diffuse

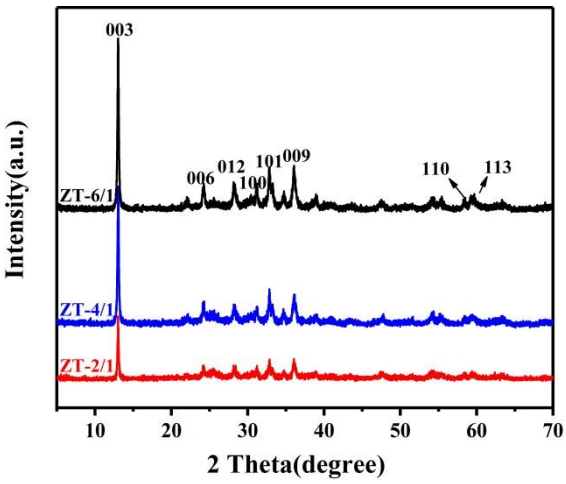

Fig. 1 Powder XRD patterns for ZnTi-LDHs.

View Article Online
DOI: 10.1039/D0CY01721C

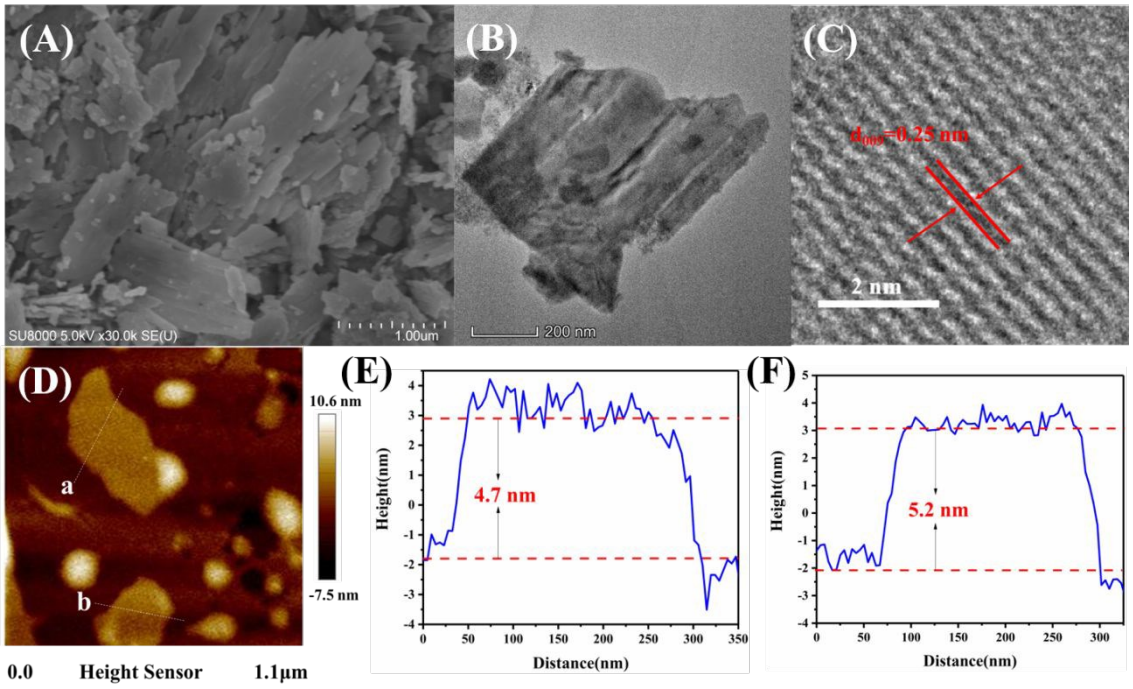

Fig. 2 FESEM image (A), TEM image (B), HRTEM image (C), AFM image (D) and the corresponding height profiles (E, F) for ZT-2/1.

reflectance spectra (UV–vis DRS) spectroscopy. UV–vis DRS and corresponding Tauc plot in Fig. S2 reveal that band gap of ZT-2/1, ZT-4/1, and ZT-6/1 are about 3.25 eV, 3.34 eV, 3.37 eV, respectively. As a result, the three ZnTi-LDHs can only respond to ultraviolet light (λ≤ 382 nm). What's more, the Mott–Schottky plots (Fig. S3) were used to measure the flat-band potentials of ZT-2/1, ZT-4/1 and ZT/6/1, which are respectively -1.1 V, -1.0 V and -0.8 V (vs. Ag/AgCl), corresponding to -0.9 V, -0.8 V and -0.6 V (vs. NHE). It is generally known that the position of conduction band (CB)is close to the flat band. And Compared with $O_2/\bullet O_2^-$ potential (-0.28 V vs. NHE), the CB of ZnTi-LDH samples are more negative. Therefore, all of them are thermodynamically permissible for reduction of O_2 to $\bullet O_2^-$, which is an important active oxygen species.

The selective photocatalytic oxidation of aniline (AL) to nitrosobenzene (NSB) was carried out over ZnTi-LDHs and P25 under visible Light (λ ≥ 400 nm) irradiation. As shown in Table 1, the conversion of AL (33.5%) with high selectivity to NSB (76.7%) was achieved over ZT-2/1 after irradiating for 4 h, which exhibited obviously superior catalytic performance than ZT-4/1 (15.4%), ZT-6/1 (8.1%) and P25(13.6%). In addition, two by-products were produced in photocatalytic reaction, including azobenzene (AB) and nitrobenzene (NB). The formation of AB, another high-value chemical, results from the condensation between AL and a part of produced NSB.[11] The NB is produced owing to the further oxidation of NSB. Table S1 summarizes photocatalytic data of aniline oxidation between the current study and reported literatures. Comparing to various photocatalysts, ZT-2/1 shows excellent photocatalytic performance on the conversion of AL and selectivity to NSB. It is worth mentioning that no product was detected under the reaction condition without ZnTi-LDH as a catalyst or in the dark condition. In addition, the photocatalytic oxidation reaction did not take place in the atmosphere of Ar. On the basis of these results, it is concluded that ZnTi-LDH, light source and oxygen are all necessary for photocatalytic oxidation of AL. Moreover, the reusability and stability of ZT-2/1 were also investigated. After the recycling of ZT-2/1 for five times, its photocatalytic activity remains stable (Fig. S4). The XRD patterns for fresh and used ZT-2/1 (Fig. S5) show no obvious change, indicating high stability of ZT-2/1. In order to explore the effect of solvents to catalytic activity, the reaction experiments using different solvents were carried out. As shown in Fig. S6, activity order is Acetonitrile > BTF > Toluene > Hexane > Ethyl Acetate > EtOH, indicating acetonitrile is the best option as the reaction solvent in this photocatalytic process. In the organic solvents without oxygen-containing functional groups, the photocatalytic conversion of aniline is improved with the increasing polarity of the solvents (acetonitrile > BTF > toluene > hexane). This is mainly because that aniline can dissolve well in the organic solvents with high polarity. In the organic solvents with oxygen-containing functional groups (ethyl acetate and EtOH), the conversion considerably decreases but the selectivity of NSB obviously increases. This result maybe contributed to the competitive adsorption of the solvent and aniline in this system.

Why the ZnTi-LDH as ultraviolet light responsive materials have catalytic performance under visible light irradiation? The

View Article Online
DOI: 10.1039/D0CY01721C

Table 1. Photocatalytic activity for the selective oxidation of aniline over ZnTi-LDHs and P25 under visible light irradiation [a].

Entry	Catalyst	Atm	Visible light (λ≥400 nm)	Conv. (%)	Sel. NSB (%)	Sel. AB (%)	Sel. NB (%)
1	ZT-2/1	O_2	+	33.5	76.7	16.1	7.2
2	ZT-2/1	O_2	–	–	–	–	–
3	None	O_2	+	–	–	–	–
4	ZT-2/1	Ar	+	–	–	–	–
5	ZT-4/1	O_2	+	15.4	79.9	13.6	6.5
6	ZT-6/1	O_2	+	8.1	86.4	6.2	7.4
7	P25	O_2	+	13.6	62.9	33.3	3.8

[a] Recation condition: aniline (0.026 mmol), catalyst (20 mg), acetonitrile (1.0 mL), temperature (25 °C), irradiation time (4 h).

optical absorption property of aniline-adsorbed ZT-2/1 (AL/ZT-2/1) was analyzed by UV–vis DRS in Fig. 3. After the absorption of AL molecules, ZT-2/1 exhibits the visible light absorption with the color change from white to yellow, as a similar phenomenon reported in our previous work.[21,25,42] This result indicates that the interaction of AL with ZT-2/1 would induce the formation of surface coordination species, which exhibited optical absorption in the visible region due to the ligand-to-metal charge transfer (LMCT).[47-49] In addition, photocurrent measurements (Fig. S7) suggest that three types of aniline-adsorbed ZnTi-LDHs have photocurrent response under visible light irradiation. AL/ZT-2/1 shows enhanced photocurrent intensity than AL/ZT-4/1 and AL/ZT-6/1, indicating that AL/ZT-2/1 has higher separation efficiency of photoelectrons. Therefore, the surface coordination active species with the property of absorption in the visible region guarantees the photocatalytic oxidation of AL under visible light irradiation.

To find out the reason why ZT-2/1 has better photocatalytic performance than other kinds of ZnTi-LDHs, a further material characterization was carried out. As shown in the FTIR spectra in Fig. 4, the intensity of the FTIR peak (3100 cm^{-1} ~ 3500 cm^{-1}) assigned to OH groups for ZT-2/1 significantly increases when compared with those for ZT-4/1, ZT-6/1 and P25, verifying that ZT-2/1 possesses a larger number of surface OH groups than the others. This is in good consistent with results of specific surface area analyzed by N_2-sorption. Consequently, it can be automatically concluded that more surface OH groups are efficiently exposed in ZT-2/1 owing to its higher specific surface area. It was demonstrated in three studies[16,43,44] that basic sites could facilitate the reductive deprotonation of AL, which was the rate determining step to oxidation of AL. Taking into account abundant OH groups on the surface of LDHs, we guess that the OH groups on ZnTi-LDHs as the Brønsted base sites could also facilitate the reductive deprotonation of AL, resulting in the excellent photocatalytic performance on oxidation of AL.

In situ FTIR analysis was further carried out to verify the interaction between ZnTi-LDH and AL molecules. As shown in Fig. 5c, after the adsorption of AL, the several peaks assigned to AL molecules appeared in the spectrum compared with that of fresh ZT-2/1. The peaks also remained even after the further evacuation (Fig. 5d), indicating that AL molecules efficiently chemisorbed on the surface of ZnTi-LDH. The peak at 1601 cm^{-1} could be ascribed to the stretching vibration of C=C ($\sigma_{C=C}$) in the aromatic ring, while the two peaks at 1174 cm^{-1} and 1152 cm^{-1} could be assigned to the stretching vibration of C-H (σ_{C-H}) in the

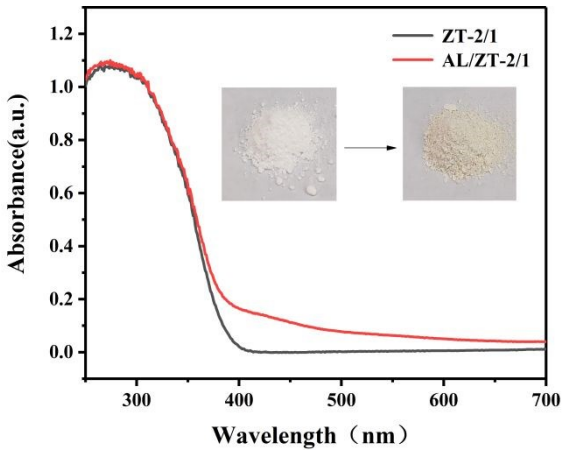

Fig. 3 UV–vis DRS spectra of ZT-2/1 and AL/ZT-2/1.

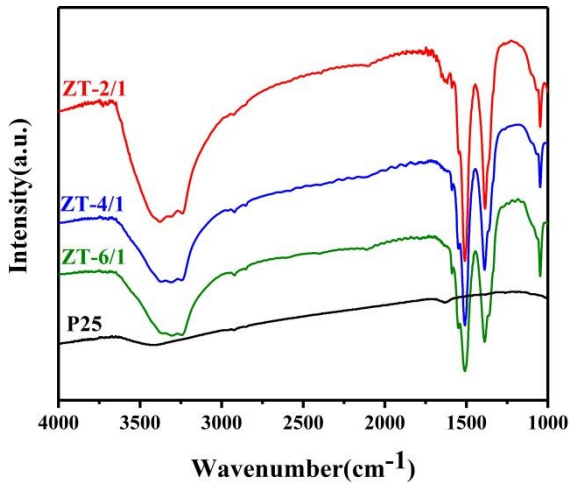

Fig. 4 FTIR spectra for ZnTi-LDHs and P25.

aromatic ring.[50] Differently, the N-H bending vibration (δ_{N-H}) at 1621cm^{-1} in the AL adsorbed onto ZT-2/1 exhibited a shift toward a higher wavenumber compared with that in free AL molecules (1618 cm^{-1}), indicating that AL molecules adsorbed onto ZT-2/1 were transformed to the new species with a stronger N−H bond.[51] It was proven in a previous study[16] that the N−H vibrational band was strengthened via deprotonation by the base. In addition, the C-N stretching vibration (σ_{C-N}) at 1277 cm^{-1} in the AL/ZT-2/1 showed a similar move. These data clearly suggest that ZT-2/1 has some kind of basic site to promote deprotonation of AL.

To further explore the active sites for the interaction between ZnTi-LDH and AL molecules, X-ray photoelectron spectroscopy (XPS) characterization was used to compare the surface properties of naked ZT-2/1 with those of AL-adsorbed ZT-2/1. As shown in Fig. 6A, Zn 2p XPS spectrum of AL/ZT-2/1 was identical to that of fresh ZT-2/1, providing the evidence of no interaction between Zn atoms and AL molecules. Nevertheless, the Ti 2p XPS spectrum of AL/ZT-2/1 in Fig. 6B

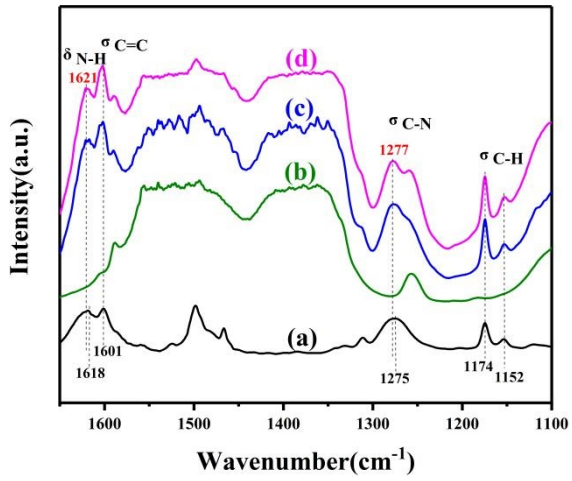

Fig. 5 In suit FTIR spectra of aniline absorption on ZT-2/1. (a) FTIR spectra of free aniline. (b) Degassing stage. (c) Physical and chemical adsorption stage. (d) Chemical adsorption stage.

exhibits a higher binding energy shift (0.1 eV) relative to the naked ZT-2/1, inferring the decrease in electron density in Ti nucleus. This result reveals the transport of electrons from Ti atoms to AL molecules after the adsorption of AL. The O 1s XPS spectra for ZT-2/1 and AL/ZT-2/1 in Fig. 6C show the three same peaks at 529.6 eV, 532.1 eV and 532.9 eV, which are attributed

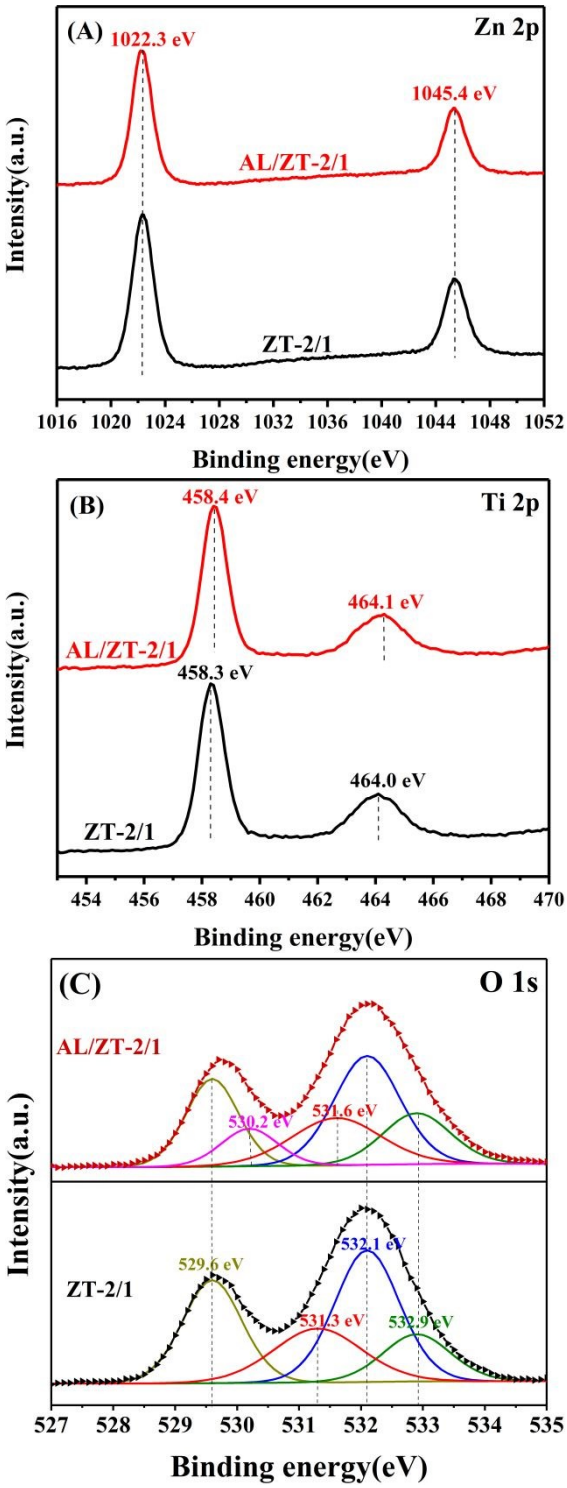

Fig. 6 The Zn 2p (A), Ti 2p (B) and O 1s (C) XPS spectra of ZT-2/1 before and after the adsorption of aniline.

to lattice oxygen, adsorbed water and C–O functional group, respectively.[52, 53] However, AL/ZT-2/1 shows a higher binding energy shift (0.3 eV) for OH groups comparing to the naked ZT-2/1 (531.3 eV), suggesting the migration of electrons from surface OH groups to AL molecules due to the adsorption of AL. Moreover, the O 1s spectrum of AL/ZT-2/1 exhibits an extra peak at 530.2 eV, which is ascribed to the adsorbed oxygen species at the vacancy sites.[54, 55] From the results we have already obtained, it can be concluded that the interaction between ZnTi-LDH and AL molecules were triggered via Ti sites and OH sites as the active sites. As a result of the interaction, surface coordination active species as well as oxygen vacancies (VOs) were formed at the same time. In addition, combining with the results of in situ FTIR analysis and abundant OH sites on LDH materials, it was further inferred that the basic site to promote deprotonation of AL was OH sites on the surface of ZT-2/1.

Subsequently, the existence of OVs in AL-adsorbed ZnTi-LDH was further confirmed by the analysis of Electron spin resonance (ESR) spectra. As shown in Fig. 7, no apparent ESR signal can be examined for the fresh ZT-2/1. On the contrary, AL/ZT-2/1 exhibited the typical ESR signal centered at g = 2.004, which was ascribed to the electrons trapped in the oxygen vacancies (OVs).[56] It was evidenced again that OVs were produced when AL molecules were adsorbed on ZT-2/1. As for AL/ZT-4/1 and AL/ZT-6/1, they exhibited obviously the weaker ESR signals, indicating formation of a smaller amount of OVs comparing to AL/ZT-2/1. Therefore, the more surface OH groups ZnTi-LDH exposed, the more OVs it could produce via the adsorption of AL molecules.

The roles of O_2 molecules in the photocatalysis reaction was evidenced by a simulated in-situ ESR measurement coupled with 5,5-dimethyl-1-pyrroline N-oxide (DMPO) as a spin trapping reagent. As shown in Fig. 8, no obvious ESR signal was detected in the absence of AL molecules or in the dark condition.

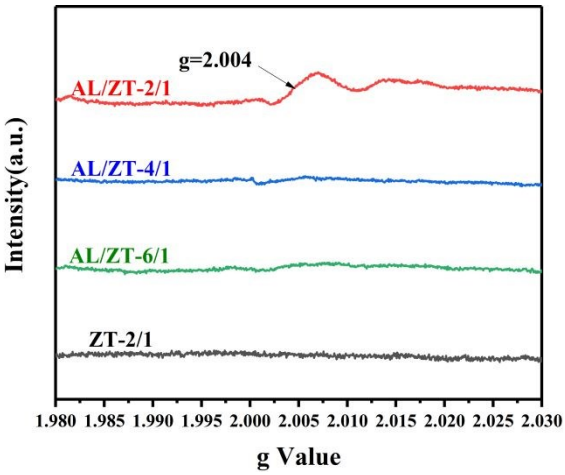

Fig. 7 ESR spectra of aniline-adsorbed ZnTi-LDHs and free ZT-2/1.

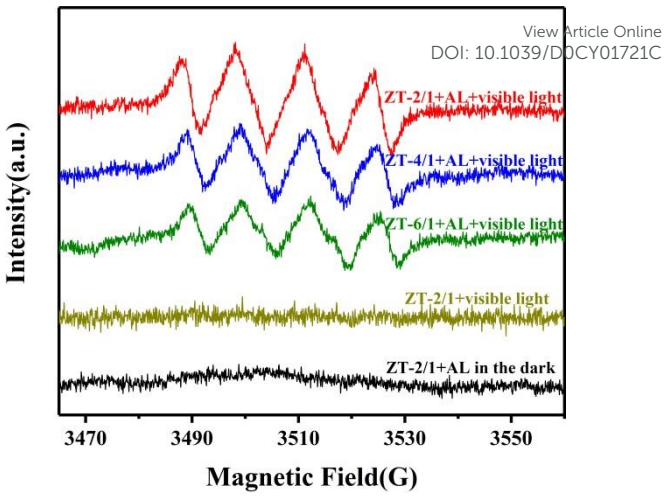

Fig. 8 DMPO trapping ESR spectra of the samples under different conditions.

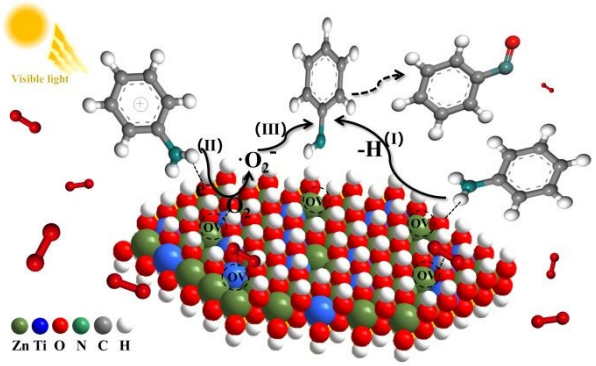

Scheme 1. Possible mechanism for selective oxidation of aniline to nitrosobenzene over ZnTi-LDH under visible light.

In contrast, ZT-2/1 with the addition of AL under visible light irradiation exhibited the typical signal assigned to the DMPO−•OOH adduct, a spin derivative of DMPO−•O_2^-, confirming the presence of •O_2^-.[55, 57] The results reveal that the generation of •O_2^- under visible light irradiation results from the surface coordination active species formed between ZnTi-LDH and AL molecules, which could absorb visible light and initiate the photocatalysis reaction. Moreover, the ESR signal intensity for ZT-2/1 is obviously stronger than those for ZT-4/1 and ZT-6/1, indicating that the ZT-2/1 possessed a superior performance to produce •O_2^- than the others after the adsorption of AL molecules. It was demonstrated in a number of studies that OVs not only serve as the centers to capture photoelectrons from the photoexcited surface coordination species, but also provide active sites to adsorption and activation of O_2.[58,59] Therefore, more OVs produced by the interaction between the ZnTi-LDH and AL molecules is definitely helpful to increase the performance to form •O_2^-, promoting photocatalytic oxidation organic reactions.

On the basis of the findings described above, a possible photocatalytic mechanism for aerobic oxidation of aniline under visible light irradiation is explained in Scheme 1. Firstly,

AL molecules are efficiently chemisorbed and activated on the surface of ZnTi-LDH via the Ti sites or OH sites as the active sites, resulting in not only forming of the surface coordination active species and OVs, but also facilitating the reductive deprotonation of AL to produce anilino species (Ⅰ). Under visible light irradiation, the surface coordination species are excited to produce photogenerated electrons, which would be captured by OVs to reduce the adsorbed and activated oxygen molecules to $\bullet O_2^-$ radicals (Ⅱ). Finally, $\bullet O_2^-$ radicals further oxidize anilino species to form the nitrosobenzene (Ⅲ).

4. Conclusions

we have prepared ZnTi-LDH nanosheets with several monolayers thickness for the selective photocatalytic aerobic oxidation of aniline to nitrosobenzene under visible light irradiation. Aniline molecules were adsorbed and activated onto the surface of ZnTi-LDH to form the surface coordination species via Ti sites or OH sites as the active sites, which could extend light absorption into the visible range and induce the photocatalytic reaction under visible light irradiation. There are two reasons to explain why the ZnTi-LDH with more exposed OH groups exhibits more excellent photocatalytic performance than the others. On the one hand, more surface OH groups as the Brønsted base sites are more beneficial to facilitate the reductive deprotonation of aniline, which is the rate determining step to oxidation of AL. On the other hand, the more OVs are formed due to the interaction between more exposed OH groups and AL molecules. As a result, more photogenerated electrons would be captured by OVs to reduce the adsorbed and activated oxygen molecules to $\bullet O_2^-$ radicals, which more effectively oxidize anilino species to form the nitrosobenzene. This work is helpful to understand the photocatalytic synthesis of nitrosobenzene at the molecular level on the basic of the interactions between catalysts and reactant molecules.

Conflicts of interest

There are no conflicts to declare.

Acknowledgements

This work was supported by the National Natural Science Foundation of China (21872032 and 51672048).

References

1 P. Zuman and B. Shah, Chem. Rev., 1994, 94, 1621-1641.
2 W. Adam and O. Krebs, Chem. Rev., 2003, 103, 4131−4146.
3 S. Meenakshisundaram, M. Selvaraju, N.M.M. Gowda and K. S. Rangappa, Int. J. Chem. Kinet., 2005, 37, 649-657.
4 B. G. Gowenlock and G. B. Richer-Addo, Chem. Rev., 2004, 104, 3315-3340.
5 A. Defoin, Synthesis, 2004, 5, 706−710.
6 S. Fountoulaki, P. L. Gkizis, T. S. Symeonidis, E. Kaminioti, A. Karina, I. Tamiolakis, G. S. Armatas and I. N. Lykakisa Adv. Synth. Catal., 2016, 358, 1500–1508.
7 S. Ghosh, S.S. Acharyya, T. Sasaki and R. Bal, Green Chem., 2015, 17, 1867–1876.
8 N.S. Kus and Monatsh. Chem., 2010, 141, 1089– 1091.
9 A. Grirrane, A. Corma and H. García, Science., 2008, 322, 1661−1664.
10 X. Lang, X. Chen and J. Zhao, Chem. Soc. Rev., 2014, 43, 473–486.
11 Z. Chai, T.T. Zeng, Q. Li, L.Q. Lu, W.J. Xiao and D. Xu, J. Am. Chem. Soc., 2016, 138, 10128–10131.
12 F. Su, S.C. Mathew, L. Mohlmann, M. Antonietti, X. Wang and S. Blechert, Angew. Chem. Int. Ed., 2011, 50, 657–660.
13 C. Karunakaran, S. Senthilvelan and S. Karuthapandian, J. Photochem. Photobiol., A 2005, 172, 207−213.
14 C. Karunakaran, S. Senthilvelan and S. Karuthapandian, Sol. Energy Mater. Sol. Cells., 2005, 89, 391−402.
15 C. Karunakaran and S. Senthilvelan, J. Mol. Catal. A: Chem, 2005, 233, 1−8.
16 Y. Shiraishi, H. Sakamoto, K. Fujiwara, S. Ichikawa and T. Hirai, ACS Catal., 2014, 4, 2418–2425.
17 Y. Sun, S. Gao, F. Lei and Y. Xie, Chem. Soc. Rev., 2015, 44, 623.
18 Y. Zheng, Y. Jiao, L. Ge, M. Jaroniec and S. Z. Qiao, Angew. Chem. Int. Ed., 2013, 52, 3110–3116.
19 Z. Yin, J. Zhu, Q. He, X. Cao, C. Tan, H. Chen, Q. Yan and H. Zhang, Adv. Energy. Mater, 2014, 4, 1300574.
20 Y. Chen, C. Tan, H. Zhang and L. Wang, Chem. Soc. Rev., 2015, 44, 2681–2701.
21 S. Liang, L. Wen, S. Lin, J. Bi, P. Feng, X. Fu and L. Wu, Angew. Chem. Int. Ed. 2014, 53, 2951–2955.
22 K. Jing, J. Xiong, N. Qin, Y. Song, L. Li, Y. Yu, S. Liang and L. Wu, Chem. Commun., 2017, 53, 8604–8607.
23 K. Jing, W. Ma, Y. Ren, J. Xiong, B. Guo, Y. Song, S. Liang and L. Wu, Appl. Catal. B Environ., 2019, 243, 10–18.
24 H. Wang, Y. Song, J. Xiong, J. Bi, L. Li, Y. Yu, S. Liang and L. Wu, Appl. Catal. B Environ., 2018, 224, 394–403.
25 Y. Song, H. Wang, X. Gao, Y. Feng, S. Liang, J. Bi, S. Lin, X. Fu and L. Wu, ACS Catal., 2017, 7, 8664–8674.
26 Y. Song, H. Wang, S. Liang, Y. Yu, L. Li and L. Wu, J. Catal., 2018, 361, 105–115.
27 Y. Song, H. Wang, Z. Wang, B. Guo, K. Jing, Y. Li and L. Wu, ACS Catal., 2018, 8, 9656−9664.
28 Y. Ren, J. Zou, K. Jing, Y. Liu, B. Guo, Y. Song, Y. Yu and L. Wu, J. Catal., 2019, 380, 123–131.
29 F. Cavani, F. Trifirb and A. Vaccari, Catal. Today., 1991, 11, 173–301.
30 Q. Wang and D. O'Hare, Chem. Rev., 2012, 112, 4124−4155.
31 L. Mohapatra and K. M. Parida, J. Mater. Chem. A, 2016, 4, 10744–10766.
32 K. M. Parida, M. Sahoo and S. Singha, J. Catal., 2010, 276, 161–169.
33 Y. Zhao, B. Li, Q. Wang, W. Gao, C. J. Wang, M. Wei, D.G. Evans, X. Duan and D. O'Hare, Chem. Sci., 2014, 5, 951–958.
34 C. G. Silva, Y. Bouizi, V. Forne´s and H. Garcı´a, J. Am. Chem. Soc., 2009, 131, 13833–13839.
35 N. Baliarsingh, L. Mohapatra and K. M. Parida, J. Mater. Chem. A, 2013, 1, 4236.
36 Y. Zhao, G. Chen, T. Bian, C. Zhou, G. I. Waterhouse, L. Z. Wu, C.H. Tung, L.J. Smith, D. O'Hare and T. Zhang, Adv. Mater, 2015, 27, 7824–7831,
37 K. Teramura, S. Iguchi, Y. Mizuno, T. Shishido and T. Tanaka, Angew. Chem. Int. Ed., 2012, 51, 8008 –8011.
38 Y. Guo, D. Li, C. Hu, Y. Wan, E. Wang, Y. Zhou and S. Feng, Appl. Catal. B Environ., 2001, 30, 337–349.
39 X. Yang, B. Chen, X. Li, L. Zheng, L. Wu and C. Tung, Chem. Commun., 2014, 50, 6664.

View Article Online
DOI: 10.1039/D0CY01721C

40 M. Sahoo, S. Mansingh and K. M. Parida, J. Mater. Chem. A, 2019, 7, 7614–7627.
41 Z. Wang, Y. Song, J. Zou, L. Li, Y. Yu and L. Wu, Catal. Sci. Technol., 2018, 8, 268–275.
42 J. Zou, Z. Wang, W. Guo, B Guo, Y. Yu and L. Wu, Appl. Catal. B Environ., 2020, 260, 118185.
43 J. Chen, J. Xiong, Y. Song, Y. Yu and L. Wu, Appl. Surf. Sci, 2018, 440, 1269–1276.
44 J. Chen, C. Shen, B. Guo, Y. Yu and L. Wu, Catal. Today, 2019, 335, 312–318.
45 M. Shao, J. Han, M. Wei, D.G. Evans and X. Duan, Chem. Eng. J, 2011, 168, 519–524.
46 O. Saber and H. Tagaya, J. Incl. Phenom. Macrocyclic Chem., 2003, 45, 109–116.
47 S. Higashimoto, K. Okada, T. Morisugi, M. Azuma, H. Ohue, T. H. Kim, M. Matsuoka and M. Anpo, Top. Catal., 2010, 53, 578–583.
48 T. Shishido, K. Teramura and T. Tanaka, Catal. Sci. Technol., 2011, 1, 541–551.
49 X. Lang, W. Ma, Y. Zhao, C. Chen, H. Ji and J. Zhao, Chem. Eur., J. 2012, 18, 2624 – 2631.
50 J. C. Evans, Spectrochim. Acta., 1960, 16, 428−442.
51 E. V. Brown and W. H. J. Kipp, Org. Chem., 1971, 36, 170−173.
52 H. Luo, B. Wang, T. Liu, F. Jin, R. Liu, C. Xu, C. Wang, K. Ji, Y. Zhou, D. Wang and S. Dou, Energy Storage Mater., 2019, 19, 370–378.
53 L. Zhang, C. Zheng, F. Li, D.G. Evans and X. Duan, J. Mater. Sci., 2007, 43, 237–243.
54 G. T. Tyuliev and K. L. Kostov, Phys. Rev. B, 1999, 60, 2900–2907.
55 H. Wang, D. Yong, S. Chen, S. Jiang, X. Zhang, W. Shao, Q. Zhang, W. Yan, B. Pan and Y. Xie, J. Am. Chem. Soc., 2018, 140, 1760–1766.
56 Q. Maqbool and A. Srivastava, Chem. Eur. J., 2017, 23, 13864–13868.
57 Y. Shiraishi, S. Kanazawa, Y. Sugano, D. Tsukamoto, H. Sakamoto, S. Ichikawa and T. Hirai, ACS Catal., 2014, 4, 774–780.
58 X. Sun, X. Luo, X. Zhang, J. Xie, S. Jin, H. Wang, X. Zheng, X. Wu and Y. Xie, J. Am. Chem. Soc., 2019, 141, 3797–3801.
59 H. Li, F. Qin, Z. Yang, X. Cui, J. Wang and L. Zhang, J. Am. Chem. Soc., 2017, 139, 3513–3521.

View Article Online
DOI: 10.1039/D0CY01721C

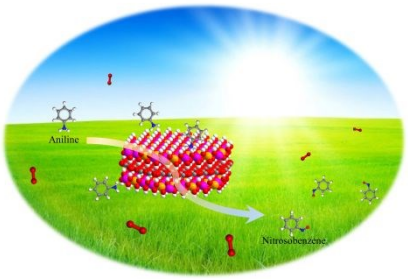

Aniline is chemisorbed and activated on ultrathin ZnTi-LDH nanosheets, facilitating photocatalytic aerobic oxidation of aniline under visible light.